Fukui Functions from the Relaxed Kohn−Sham Orbitals

A. Michalak,[†] F. De Proft,[‡] P. Geerlings,[‡] and R. F. Nalewajski*[,§]

Department of Computational Methods in Chemistry, Jagiellonian University, R. Ingardena 3, 30-060 Cracow, Poland, Eenheid Algemene Chemie, Vrije Universiteit Brussel, Pleinlaan 2, B-1050 Brussels, Belgium, and K. Gumiński Department of Theoretical Chemistry, Jagiellonian University, R. Ingardena 3, 30-060 Cracow, Poland

Received: June 24, 1998; In Final Form: October 2, 1998

The global Fukui function of a molecular system, $f(\mathbf{r}) = (\partial\rho(\mathbf{r})/\partial N)_v$, where ρ is the ground-state density of a system containing N electrons moving in the external potential $v(\mathbf{r})$, is calculated within a single Kohn−Sham calculation. It is determined by adding to the rigid (frontier orbital) term, relevant for the electron removal ($dN < 0$) or addition ($dN > 0$), the density relaxation contribution determined from the N-differentiated Kohn−Sham equations. The only approximation introduced is a neglect of the exchange−correlation terms in the N-derivative of the effective one-body potential. The corresponding equations resulting from the basis set expansion of orbitals are derived, and illustrative results for CO, HCN, H_2CO are reported. The predicted Fukui functions for pyrrole, furane, and tiophene are used to diagnose reactivity toward an electrophilic attack. The contour maps of $f(\mathbf{r})$ and the resulting condensed Fukui function indices are compared with the corresponding $|\Delta N| = 1$ and the "exact" $|\Delta N| \rightarrow 0$ finite difference predictions.

1. Introduction

The *Fukui function* (FF)[1−4] and related hardness/softness characteristics[2−10] constitute the major chemical descriptors of molecular species as open systems, in which the number of electrons N represents the continuous equilibrium state variable.[11] As such, they constitute important reactivity criteria[2−4,9,10] and give rise to corresponding contributions to the interaction energy between reactants.[2,3] In the frozen core approximation FF represents the density of the relevant frontier molecular orbital involved in electron receiving (*nucleophilic attack*) or withdrawing (*electrophilic attack*) processes.[1] Besides the local functions corresponding to the global equilibrium in the molecule as a whole, when the local electronegativities are equalized throughout the system,[12,13] the 2×2 matrix of the FF-type quantities[3,14−16] is required to describe the electron redistribution in the intermediate, constrained equilibrium of the reactive system, when the charge transfer between reactants is not permitted (so-called polarized reactant stage); the electronegativity equalization is then limited only to each reactant. The relevant FF then allows one to combine the local chemical potential or hardness derivatives into the corresponding global/regional quantities corresponding to the type of equilibrium under consideration.[3,10,17,18] Within the charge sensitivity analysis[3,9,10,19] and the related electronegativity equalization method[20] the FF and their atomic indices are widely used to explore reactivity trends of large molecular systems.[3,9,10,16]

The theory and algorithms for determining the local and condensed FF data are still being developed.[2−4,10,14−17,21−27] The most common is the finite difference approach proposed by Parr and Yang,[1] in which the separate *nucleophilic* (for an electron inflow to the system from a nucleophilic environment), *electrophilic* (for an electron outflow from the system to the electrophilic agent), and *average* (isoelectronic, to be applied in a case of a radical attack) *FF* are determined from independent molecular orbital calculations for the neutral and the two ionic species. Both physical space[23] and orbital space partitionings[1] of corresponding density differences can be used to determine the relevant condensed atomic FF indices from local functions.[28] They can also be calculated directly within the charge sensitivity analysis from the hardnes matrix in atomic resolution via the electronegativity equalization equations.[3,9,10,14−16,19] The single spin-polarized Kohn−Sham calculations can also be used to obtain FF from the Taylor expansion of spin densities at the spin nonpolarized point.[21] The variational principle for the FF,[24] in terms of the global hardness functional, has also been used to determine FF;[26] the underlying local hardness equalization principle is a direct consequence of the electronegativity equalization.[3,29] Recently, several algorithms have been proposed, which explicitly use the derivatives of the molecular orbitals with respect to the global number of electrons.[18a,22,25,27] For example, the differential orbital relaxation, due to an infinitesimal shift in the number of electrons, can be determined from the N-differentiated Kohn−Sham equations.[18a,25] The present work presents the first practical implementation of this strategy.

As we have already remarked, the FF itself, by not being linked directly to the overall change in the system energy due to a hypothetical attack by another agent, can only serve as a qualitative reactivity criterion. Therefore, approximate but realistic estimates of this function can perform equally well as more exact ones in diagnosing reactivity trends. To make it applicable to very large systems, the differential algorithm for generating FF should not be dramatically more time-consuming than the standard Hartree−Fock or Kohn−Sham scheme, for example, by requiring the same set of electron repulsion integrals in a given basis set. This requirement is met within the present

* Corresponding author.
[†] Department of Computational Methods in Chemistry, Jagiellonian University.
[‡] Vrije Universiteit Brussel.
[§] K. Gumiński Department of Theoretical Chemistry, Jagiellonian University.

10.1021/jp982761i CCC: $18.00
Published on Web 01/22/1999

algorithm, in which the Kohn−Sham (correlated) frontier orbital density is modified by the approximate density relaxation term, obtained by neglecting the *N*-derivative of the exchange−correlation potential in the *N*-derivative of the effective one-body potential. The adequacy of such an approach is tested on a number of small molecules that were previously studied by other methods. The calculated FF maps are compared with the corresponding standard and modified finite difference results. The reactivity predictions for an electrophilic attack on selected five-membered heterocycles are compared with the experimentally determined α-preference of such substitution reactions. The relevance of the most common Mulliken-type atomic discretization of the FF into condensed indices is examined and discussed.

2. Theoretical Background

Global *Fukui function*[1−4] of a molecule M as a whole measures the response of its ground-state electron density, $\rho(\mathbf{r})$, per unit shift in the system number of electrons, *N*, for constant external potential due to the nuclei, $v(\mathbf{r})$:

$$f(\mathbf{r}) = \left(\frac{\partial \rho(\mathbf{r})}{\partial N}\right)_v \tag{1}$$

As such, it characterizes an open system in contact with a hypothetical external electron reservoir *R* specified by the value of its chemical potential $\mu_R = \mu = (\partial E/\partial N)_v$, where $E = E[N,v]$ is the ground-state energy of M. Also, by the Maxwell relation,[1,30] this function monitors the response in μ per unit displacement in the local value of the external potential, for constant (ensemble) average number of electrons:

$$f(\mathbf{r}) = \left(\frac{\delta \mu}{\partial v(\mathbf{r})}\right)_N \tag{2}$$

In what follows we shall use the first definition. To simplify notation, the v constraint will not be explicitly indicated; atomic units will be used throughout the paper.

In the *Kohn−Sham* (KS) scheme[31] of the density functional theory,[32] the electron distribution is generated from the KS *molecular orbitals* (MO), $|\varphi\rangle = |\varphi_1, \varphi_2, ...\rangle \equiv \{|x\rangle\}$:

$$\rho(\mathbf{r}) = |\varphi\rangle \mathbf{n} \langle\varphi| = \sum_x^{\text{occ}} n_x |\varphi_x(\mathbf{r})|^2 \tag{3}$$

satisfying the familiar KS equations, $\hat{h}_{\text{KS}}\varphi_x = e_x\varphi_x$. Here, $\hat{h}_{\text{KS}}(\mathbf{r}) = -(1/2)\Delta + v_{\text{KS}}(\mathbf{r})$ is the KS hamiltonian and $\{e_x\}$ stands for a set of its eigenvalues. This one-electron operator is defined by the effective one-body potential $v_{\text{KS}}(\mathbf{r})$ including the Hartree and exchange−correlation terms. The MO set consists of vectors of the *occupied* (o) and *virtual* (v) orbitals: $|\varphi\rangle = |\varphi_o, \varphi_v\rangle$. The nonvanishing elements of the diagonal matrix of orbital occupations $\mathbf{n} = \{n_x\delta_{xx'}\}$ are in the unit matrix $\mathbf{I}_{oo}$ corresponding to occupied orbitals:

$$\mathbf{n} = \begin{pmatrix} \mathbf{I}_{oo} & \mathbf{0}_{ov} \\ \mathbf{0}_{v,o} & \mathbf{0}_{vv} \end{pmatrix} \tag{4}$$

Denoting the *N*-differentiation by a prime, one obtains from eq 3 the following expression:

$$\begin{aligned} f(\mathbf{r}) &= |\varphi\rangle \mathbf{n}' \langle\varphi| + [|\varphi'\rangle \mathbf{n} \langle\varphi| + |\varphi\rangle \mathbf{n} \langle\varphi'|] \\ &\equiv f^F(\mathbf{r}) + [f^R(\mathbf{r})] \end{aligned} \tag{5}$$

in which the first ("frontier") term corresponds to the "frozen" shapes of orbitals and the remaining part is due to the orbital relaxation. The frontier contribution is due to a displacement in the relevant frontier orbital occupation, $dN = dn_F$:

$$f^F(\mathbf{r}) = |\varphi\rangle \mathbf{n}' \langle\varphi| = |\varphi_F(\mathbf{r})|^2 \qquad F = \text{HOMO, LUMO} \tag{6}$$

where $\mathbf{n}' = \{(\partial n_x/\partial N)\delta_{xx'} = \delta_{xF}\}$; here, the *highest occupied* (HO) and *lowest unoccupied* (LU) MO are involved in the electron outflow ($dN < 0$, chemical oxidation) and the electron inflow ($dN > 0$, chemical reduction) displacements, respectively.

To evaluate the relaxational part, $f^R(\mathbf{r})$, one needs the *N*-derivatives of the KS orbitals. When they are expressed as linear combinations of all (occupied and virtual) orbitals,

$$|\varphi'\rangle = |\varphi\rangle \mathbf{G} \equiv \{|x'\rangle\} \tag{7}$$

where, by the orthogonality relation between $|x\rangle$ and $|x'\rangle$, $G_{xx} = 0$,

$$\begin{aligned} f^R(\mathbf{r}) &= |\varphi\rangle \mathbf{G}\mathbf{n} \langle\varphi| + |\varphi\rangle \mathbf{n}\mathbf{G}^\dagger \langle\varphi| \\ &= |\varphi\rangle (\mathbf{G}\mathbf{n} + \mathbf{n}\mathbf{G}^\dagger) \langle\varphi| \end{aligned} \tag{8}$$

Let us partition the matrix $\mathbf{G} = \langle\varphi|\varphi'\rangle = \langle\varphi_o, \varphi_v|\varphi'_o, \varphi'_v\rangle$ into blocks corresponding to occupied and virtual orbitals:

$$\mathbf{G} = \begin{pmatrix} \langle\varphi_o|\varphi'_o\rangle & \langle\varphi_o|\varphi'_v\rangle \\ \langle\varphi_v|\varphi'_o\rangle & \langle\varphi_v|\varphi'_v\rangle \end{pmatrix} \equiv \begin{pmatrix} \mathbf{G}_{oo} & \mathbf{G}_{ov} \\ \mathbf{G}_{vo} & \mathbf{G}_{vv} \end{pmatrix} \tag{9}$$

An expansion of molecular orbitals in the generally nonorthogonal basis set $|\chi\rangle = |\chi_1, \chi_2, ...\rangle$, say the *atomic orbitals* (AO),

$$|\varphi\rangle = |\chi\rangle \mathbf{C} \tag{10}$$

where and $\mathbf{C} = \mathbf{S}^{-1}\langle\chi|\varphi_o, \varphi_v\rangle \equiv [\mathbf{C}_o, \mathbf{C}_v]$ and $\mathbf{S}^{-1}$ is the inverse of the overlap matrix $\mathbf{S} = \langle\chi|\chi\rangle$, allows one to write the frontier and relaxational parts of the FF as combinations of products of basis functions:

$$f^F(\mathbf{r}) = |\chi\rangle \mathbf{C}\mathbf{n}'\mathbf{C}^\dagger \langle\chi| \equiv |\chi\rangle \mathbf{F}^F \langle\chi| \tag{11}$$

$$f^R(\mathbf{r}) = |\chi\rangle \mathbf{C}(\mathbf{G}\mathbf{n} + \mathbf{n}\mathbf{G}^\dagger)\mathbf{C}^\dagger \langle\chi| \equiv |\chi\rangle \mathbf{F}^R \langle\chi| \tag{12}$$

These equations define the basis set matrix representations $\mathbf{F}^F$ and $\mathbf{F}^R$ of the underlying rigid and relaxed FF operators.

Thus, the resultant FF in the atomic orbital basis set is

$$f(\mathbf{r}) = |\chi\rangle \mathbf{F} \langle\chi| = \sum_k^{\text{AO}} \sum_l^{\text{AO}} F_{kl} \chi_k^*(\mathbf{r}) \chi_l(\mathbf{r}) \tag{13}$$

where the overall *Fukui function matrix* $\mathbf{F} = \mathbf{F}^F + \mathbf{F}^R$. A comparison between eq 13 and the basis set expression for the electron density,

$$\rho(\mathbf{r}) = |\chi\rangle \mathbf{P} \langle\chi| = \sum_k^{\text{AO}} \sum_l^{\text{AO}} P_{kl} \chi_k^*(\mathbf{r}) \chi_l(\mathbf{r}) \tag{14}$$

where the *charge-and-bond-order* (CBO) matrix $\mathbf{P} = \mathbf{C}\mathbf{n}\mathbf{C}^\dagger$, identifies $\mathbf{F}$ as the *N*-derivative of $\mathbf{P}$:

$$\mathbf{F} = \partial \mathbf{P}/\partial N \tag{15}$$

The molecular FF must be normalized: $\int f(\mathbf{r})\, d\mathbf{r} = \partial N/\partial N = 1$. Following the Mulliken populational analysis, this integral can be partitioned into the condensed FF indices, $\{f_A\}$, of *atoms-*

in-molecules (AIM):

$$\int f(\mathbf{r})\,d\mathbf{r} = \mathrm{tr}(\mathbf{FS}) = \sum_{\mathrm{A}}^{\mathrm{AIM}}\Big(\sum_{i\in\mathrm{A}}^{\mathrm{AO}}(\mathbf{FS})_{ii}\Big) \equiv \sum_{\mathrm{A}}^{\mathrm{AIM}} f_{\mathrm{A}} = 1 \quad (16)$$

Obviously, the same expression for the $\{f_{\mathrm{A}}\}$ results from the *N*-differentiation of the Mulliken AIM populations $\{N_{\mathrm{A}} = \sum_{i\in\mathrm{A}}^{\mathrm{AO}}(\mathbf{PS})_{ii}\}$.

In order to determine the **G** matrix of eq 7, the *N*-differentiated KS equations[18a,25]

$$(\hat{h}_{\mathrm{KS}} - e_x)\frac{\partial\varphi_x}{\partial N} = \left(\frac{\partial e_x}{\partial N} - \frac{\partial v_{\mathrm{KS}}}{\partial N}\right)\varphi_x \quad (17)$$

are used. In this approach

$$G_{xx'} = \frac{\langle\varphi_x|v'_{\mathrm{KS}}|\varphi_{x'}\rangle}{e_{x'} - e_x} \quad (18)$$

where $v'_{\mathrm{KS}}(\mathbf{r}) \equiv \partial v_{\mathrm{KS}}(\mathbf{r})/\partial N$ and

$$v_{\mathrm{KS}}(\mathbf{r}) = v(\mathbf{r}) + \int\frac{\rho(\mathbf{r}')}{|\mathbf{r}-\mathbf{r}'|}\,d\mathbf{r}' + v_{\mathrm{XC}}(\mathbf{r}) \equiv v_{\mathrm{H}}(\mathbf{r}) + v_{\mathrm{XC}}(\mathbf{r}) \quad (19)$$

Here, v_{H} and v_{XC} stand for the Hartree and exchange−correlation potentials, respectively.

Since the frontier $f^F(\mathbf{r})$ part in eq 5 already includes some exchange−correlation effects, we believe that a workable scheme for generating realistic FF, adequate for qualitative reactivity predictions, is to simplify eq 17 for determining *N*-derivatives of the KS orbitals, giving rise to the relaxational $f^{\mathrm{R}}(\mathbf{r})$ component. We would like to emphasize that each of the four terms of eq 17 has some exchange−correlation content. However, when one neglects the exchange−correlation contribution in one of them, viz., in the *N*-derivative of v_{KS},

$$v'_{\mathrm{KS}}(\mathbf{r}) \approx \partial v_{\mathrm{H}}(\mathbf{r})/\partial N = \frac{\partial}{\partial N}\int\frac{\rho(\mathbf{r}')}{|\mathbf{r}-\mathbf{r}'|}\,d\mathbf{r}'$$

$$= \int\frac{f(\mathbf{r}')}{|\mathbf{r}-\mathbf{r}'|}\,d\mathbf{r}' = \sum_{m}^{\mathrm{AO}}\sum_{n}^{\mathrm{AO}}F_{mn}\int\frac{\chi^*_m(\mathbf{r}')\chi_n(\mathbf{r}')}{|\mathbf{r}-\mathbf{r}'|}\,d\mathbf{r}' \quad (20)$$

the required two-electron integrals do not go beyond those needed in the standard SCF/KS calculations and one determines the relaxed orbital expansion coefficients of eq 7 from a set of linear equations that can be solved directly. Including the *N*-derivative of the exchange correlation potential in eqs 17 and 18 would greatly complicate the algorithm by necessary numerical integration and an iterative procedure for determining the orbital relaxation part of the FF. Such a scheme would severely limit the range of applications of differential FF as a diagnostic reactivity criterion for large systems. For this reason only, we adopt the approximation of eq 20 in the present algorithm, the complexity of which thus becomes comparable to that of a single SCF/KS run. Such a differential approach has an additional advantage of avoiding the slowly convergent electronic structure calculations for negative ions, which are necessary in the finite difference approximation.

Hence, the **G** matrix can be expressed in terms of the unknown FF matrix **F**:

$$G_{xx'} = \epsilon_{xx'}\sum_{i}^{\mathrm{AO}}\sum_{j}^{\mathrm{AO}}C^*_{ix}C_{jx'}\sum_{m}^{\mathrm{AO}}\sum_{n}^{\mathrm{AO}}F_{mn}(\chi_i\chi_j|\chi_m\chi_n) \quad (21)$$

where $\epsilon_{xx'} = 1/(e_{x'} - e_x)$ and the two-electron repulsion integrals in the AO basis set $(\chi_i\chi_j|\chi_m\chi_n) = \int\int\chi^*_i(\mathbf{r}')\chi_j(\mathbf{r}')|\mathbf{r} - \mathbf{r}'|^{-1}\chi^*_m(\mathbf{r})\chi_n(\mathbf{r})\,d\mathbf{r}\,d\mathbf{r}'$.

Expressing $\mathbf{F}^{\mathrm{R}}$ in terms of the corresponding o/v MO components (see eqs 4 and 9) gives

$$\mathbf{F}^{\mathrm{R}} = \mathbf{C}\begin{bmatrix}\mathbf{G}_{\mathrm{oo}} + \mathbf{G}_{\mathrm{oo}}{}^{\dagger} & \mathbf{G}_{\mathrm{vo}}{}^{\dagger}\\ \mathbf{G}_{\mathrm{vo}} & \mathbf{0}_{\mathrm{vv}}\end{bmatrix}\mathbf{C}^{\dagger} = \mathbf{C}_{\mathrm{v}}\mathbf{G}_{\mathrm{vo}}\mathbf{C}_{\mathrm{o}}{}^{\dagger} + \mathbf{C}_{\mathrm{o}}\mathbf{G}_{\mathrm{vo}}{}^{\dagger}\mathbf{C}_{\mathrm{v}}^{\dagger} \quad (22)$$

since (see eq 7, 18) $\mathbf{G}_{\mathrm{oo}} + \mathbf{G}_{\mathrm{oo}}{}^{\dagger} = \mathbf{0}_{\mathrm{oo}}$. Indeed, the density relaxation due to the d*N* displacement results only from that part of the relaxed occupied MO, which is represented by the virtual orbital component; the other part of the relaxed occupied MO represents mixing of the occupied orbitals among themselves, which has no effect upon the ground-state electron density.

Therefore, the matrix element F^{R}_{kl} is given by the following summations involving pairs of occupied and virtual MO (see eq 21):

$$F^{\mathrm{R}}_{kl} = \sum_{x}^{\mathrm{virt}}\sum_{x'}^{\mathrm{occ}}G_{xx'}(C_{kx'}C^*_{lx} + C^*_{kx}C_{lx'})$$

$$= \sum_{m}^{\mathrm{AO}}\sum_{n}^{\mathrm{AO}}\Big[\sum_{x}^{\mathrm{virt}}\sum_{x'}^{\mathrm{occ}}\epsilon_{xx'}n_{x'}(C_{kx'}C^*_{lx} + C^*_{kx}C_{lx'}) \times \sum_{i}^{\mathrm{AO}}\sum_{j}^{\mathrm{AO}}C^*_{ix}C_{jx'}(\chi_i\chi_j|\chi_m\chi_n)\Big]F_{mn}$$

$$\equiv \sum_{m}^{\mathrm{AO}}\sum_{n}^{\mathrm{AO}}B_{kl,mn}F_{mn} \quad (23)$$

The resulting system of equations

$$\mathbf{F} - \mathbf{F}^{\mathrm{R}}(\mathbf{F}) = \mathbf{F}^{F} \quad (24)$$

for the unknown, linearly independent matrix elements $F_{mn}(m \le n)$ of the symmetric matrix **F** (see eqs 11 and 12) is

$$\sum_{m\le}^{\mathrm{AO}}\sum_{n}^{\mathrm{AO}}A_{kl,mn}F_{mn} = F^F_{kl}, \quad k \le l \quad (25)$$

where

$$A_{kl,mn} = (B_{kl,mn} - \delta_{km}\delta_{ln})(\delta_{mn} - 2) \quad (26)$$

The practical implementation of this scheme involves a single Kohn−Sham calculation of orbitals; for this purpose we have used the standard DeMon[33] software. The four-index electron repulsion integrals have been calculated in the Gaussian basis set using the integral package of the GAMESS[34] program.

3. Finite Difference Estimates

The local FF from eqs 13 and 25 will be compared with the commonly used *finite difference* (fd) approximation:[1]

$$f(\mathbf{r}) \approx f_{\mathrm{fd}}(\mathbf{r}) = \frac{\rho(\mathbf{r};N_0+\Delta N) - \rho(\mathbf{r};N_0)}{\Delta N} \quad (27)$$

where $\Delta N = \pm 1$, which requires three KS calculations for the nuetral and two ionic species, respectively. The numerical convergence of the generalized finite difference expression for the fractional $|\Delta N| < 1$ to the "exact" FF,

$$f(\mathbf{r}) = \lim_{\Delta N \to 0} \frac{\rho(\mathbf{r};N_0+\Delta N) - \rho(\mathbf{r};N_0)}{\Delta N} \tag{28}$$

which includes the contribution due to the N-derivative of the exchange−correlation potential, will also be examined and compared with our approximate relaxed orbital predictions, which neglect this effect. A similar comparison will be presented for the condensed FF indices of AIM,$\{f_A\}$ (from eq 16).

In order to examine the structure and hierarchy of various contributions to the finite difference FF of eq 27, let us define the changes in the shapes of orbitals,

$$\varphi_{fd}(\mathbf{r};N_0+\Delta N) \equiv \varphi(\mathbf{r};N_0) + \Delta\varphi(\mathbf{r};\Delta N) \tag{29}$$

and their occupations,

$$\mathbf{n}_{fd}(N_0+\Delta N) \equiv \mathbf{n}(N_0) + \Delta\mathbf{n}(\Delta N) \tag{30}$$

corresponding to the assumed displacement ΔN; here, $\Delta\mathbf{n} \equiv \{\Delta n_F = \Delta N \text{ and } \Delta n_{x\neq F} = 0\}$. Hence, (see eq 3) the displaced ground-state electron density

$$\rho_{fd}(\mathbf{r};N_0+\Delta N) \equiv \rho(\mathbf{r};N_0) + \Delta\rho(\mathbf{r};\Delta N)$$
$$= |\varphi_{fd}(\mathbf{r};N_0+\Delta N)\rangle \mathbf{n}_{fd}(N_0+\Delta N)\langle\varphi_{fd}(\mathbf{r};N_0+\Delta N)| \tag{31}$$

gives rise to the corresponding terms in the finite difference FF (eq 27):

$$f_{fd}(\mathbf{r}) = \frac{1}{\Delta N}\{[|\varphi(\mathbf{r})\rangle\Delta\mathbf{n}\langle\varphi(\mathbf{r})| + |\Delta\varphi(\mathbf{r})\rangle\mathbf{n}\langle\varphi(\mathbf{r})| +$$
$$|\varphi(\mathbf{r})\rangle\mathbf{n}\langle\Delta\varphi(\mathbf{r})|] + |\Delta\varphi(\mathbf{r})\rangle\Delta\mathbf{n}\langle\varphi(\mathbf{r})| + |\varphi(\mathbf{r})\rangle\Delta\mathbf{n}\langle\Delta\varphi(\mathbf{r})| +$$
$$|\Delta\varphi(\mathbf{r})\rangle\mathbf{n}\langle\Delta\varphi(\mathbf{r})| + |\Delta\varphi(\mathbf{r})\rangle\Delta\mathbf{n}\langle\Delta\varphi(\mathbf{r})|\} \tag{32}$$

including contributions of the first, second, and third order, in terms of the orbital/occupation displacements, respectively.

Only the linear part of the above expression (in brackets) involves uniquely defined fd N-derivatives of MO and their occupations:

$$f_{fdlin}(\mathbf{r}) = |\varphi(\mathbf{r})\rangle\frac{\Delta\mathbf{n}}{\Delta N}\langle\varphi(\mathbf{r})| + \left|\frac{\Delta\varphi(\mathbf{r})}{\Delta N}\right\rangle\mathbf{n}\langle\varphi(\mathbf{r})| +$$
$$|\varphi(\mathbf{r})\rangle\mathbf{n}\left\langle\frac{\Delta\varphi(\mathbf{r})}{\Delta N}\right| \tag{33}$$

For a finite ΔN this function should therefore constitute a more natural fd expression, which exhibits exactly the same structure of derivatives as the differential FF of eq 5. It remains to be seen how strongly the higher-order terms in $f_{fd}(\mathbf{r})$ distort the local features of this first-order part, particularly for $\Delta N = \pm 1$. In the present work we shall examine this effect in some detail.

It should be emphasized that the differential FF does not include a contribution due to the relaxation of LUMO, since its occupation vanishes for the configuration, for which the derivative is calculated (see eqs 4 and 5). Clearly, such second-order terms,

$$f^R_{LUMO}(\mathbf{r}) = |\varphi_{LUMO}\rangle\Delta N\langle\varphi_{LUMO}| + |\varphi_{LUMO}\rangle\Delta N\langle\varphi_{LUMO}| \tag{34}$$

are present in the finite $\Delta N > 0$ estimate, since LUMO is populated in the anion.

Owing to the discontinuity of the Fukui function,[4,11] the left- and right-side N-derivatives, $f^-(\mathbf{r})$ and $f^+(\mathbf{r})$, are introduced.[1] They correspond to the (dN, ΔN) < 0 and (dN, ΔN) > 0, respectively; in other words, the plus (minus) superscript of the FF symbol refers to the electron addition (removal) displacement in the defining derivative. In the finite difference approximation the two derivatives are distinguished by the sign of ΔN, while in the present (differential) approach the choice of the rigid part (HOMO or LUMO density) uniquely classifies the character of the right or left N-derivatives of the electron density.

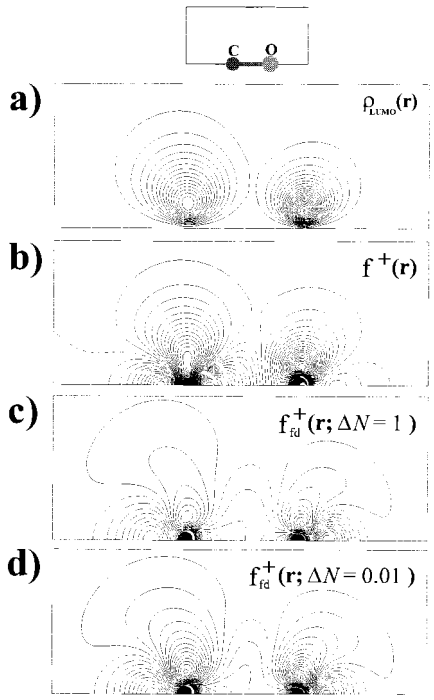

Figure 1. Comparison of the local $f^+(\mathbf{r})$ FF for CO. The first two panels correspond to the frontier (a) and overall (b) FF contour maps obtained from the present approach, while the two remaining panels report the finite difference diagrams for $\Delta N = 1$ (c) and $\Delta N = 0.01$ (d). Solid (dashed) lines correspond to the positive (negative) equidistant contour values; they are separated by the $f^+(\mathbf{r}) = 0$ contour (short-dashed line). The contour increment is 0.005 au. The same convention is used in Figures 2−5, 7, and 9−11.

4. Illustrative Applications

We have selected six molecules, carbon monoxide, hydrogen cyanide, formaldehyde, pyrrole, furane, and tiophene to test the accuracy of the approximation adapted in the present work. The set of three small molecules exhibits the localized antibonding π orbital as LUMO and the delocalized σ orbital of increasing size as HOMO. Pyrrole, furane, and tiophene have been selected to test whether both local and condensed FF data, treated as reactivity criteria, correctly predict the known preference for the electrophilic substitution on the α carbon. We have deliberately selected the set of molecules in which both the single and fractional electron displacements refer to a change in occupation of the frontier orbital only, in order to facilitate a comparison between various approximations. However, in a general case one can expect the single-electron displacement in the number of electrons to modify occupations of other orbitals as well; such a rearrangement would generate a larger nonlinear part of the finite difference FF pattern relative to the differential one.

In Figures 1−12 we have compared plots of the local FF contour maps and their profiles, obtained from various approaches and approximations for CO (Figures 1 and 2), HCN (Figures 3 and 4), H_2CO (Figures 5−10), pyrrole (Figure 11 and 12), and furane and tiophene (Figure 12). They include both the differential estimates of the present approach and the finite

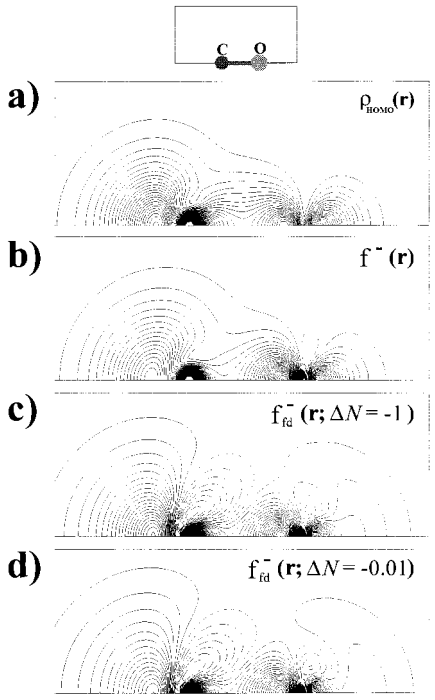

Figure 2. $f^-(\mathbf{r})$ FF contour maps for CO.

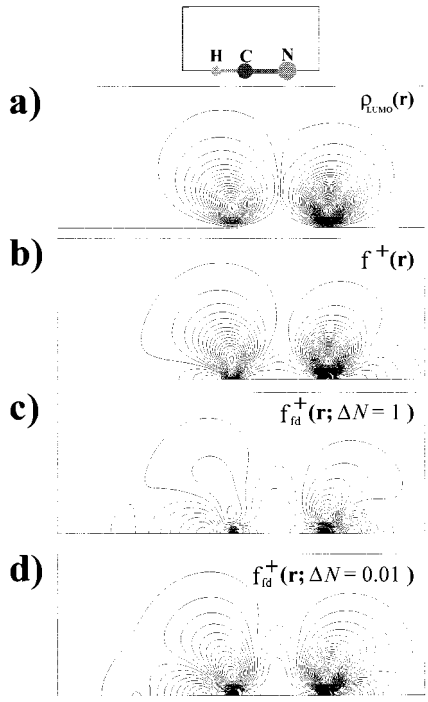

Figure 3. $f^+(\mathbf{r})$ FF contour diagrams for HCN.

difference predictions corresponding to the single and fractional displacements in the number of electrons. The representative plots of the first-order part of the finite difference FF, $f_{fdlin}(\mathbf{r})$, for the neutral formaldehyde are shown in parts a and b of Figure 9 and Figure 10. In addition the FF for an electron withdrawal from the H_2CO^- is shown in Figure 9c.

The discrete atomic FF indices obtained from the Mulliken population analysis (eq 16) are listed in Table 1. All calculations refer to the LSDA-optimized geometries in the standard DZVP extended basis sets for all constituent atoms.

Differential Fukui Functions. Within the orbital approximation (Hartree−Fock or KS theories) the LUMO corresponds to the HOMO of the $N_0 + 1$ electron system (anion M^-). In the

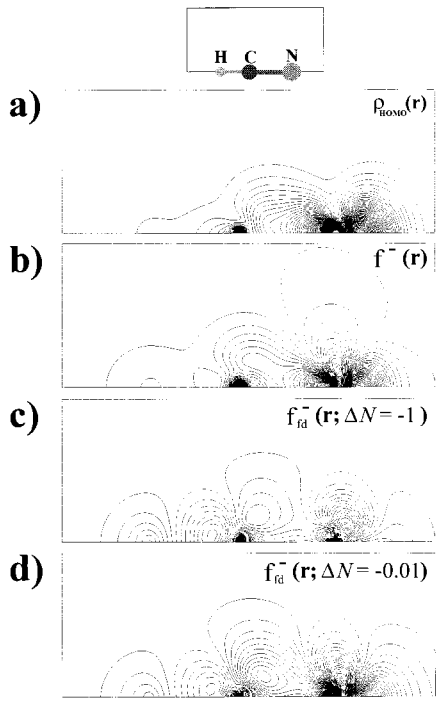

Figure 4. $f^-(\mathbf{r})$ FF contours for HCN.

ground state of CO, HCN, and H_2CO the LUMO is identified as the antibonding π^* orbital, the density of which (the rigid nucleophilic FF) is shown in panels a of Figures 1, 3 and 5. A reference to panels b of the figures shows that the orbital relaxation mixes the frontier π^* orbital with all occupied MO. In particular the σ orbital components can be clearly detected in the differential f^+ contour diagrams. Note that the π and σ contributions act with the opposite phases in the resultant (nucleophilic) FF. A stronger $\sigma-\pi$ polarization is also present in the remaining panels of the figures showing the finite difference f^+ maps. It is seen that an addition of an electron or its fraction to the LUMO indeed weakens the multiple bonds in these molecules, since it lowers the electron density in the bonding regions of the σ and π electrons.

The corresponding electrophilic FF plots (f diagrams) are shown in Figures 2, 4 and 7. The changes between the differential FF (panels b) and the HOMO densities (rigid FF, panels a) are seen to be relatively small for CO; in the HCN case one detects a much stronger negative feature on nitrogen because of an admixture of π orbitals. Still larger effects are observed in the remaining (finite difference) plots. The differential FF plot of Figure 7b indicates that the orbital relaxation diminishes the H component of f in comparison to ρ_{HOMO}, thus making the oxygen lone pair the dominant feature of Figure 7b. This is in sharp contrast to the finite difference maps predicting a strong participation of the hydrogen densities in the relaxed pattern for an electron removal. A reference to parts b−d of Figure 7 also shows that the orbital relaxation lowers the density in the bonding regions; this effect is again much stronger in the fd plots, where the hydrogen electrons become less bonding in comparison to the frontier density diagram of panel a.

A comparison of the electrophilic FF plots for pyrrole, shown in Figure 11, leads to similar conclusions. The rigid, frontier component, shown in panel a, is the $C_\alpha-C_\beta$ π bonding MO, which acquires in the differential diagram of panel b a small nitrogen π component as a result of the orbital relaxation. There is basically no σ component in the differential FF; the finite difference approach (panels c and d) produces a higher degree

TABLE 1: Differential and Finite Difference Estimates of the Atomic FF Indices for CO, HCN, H_2CO, Pyrrole, Furane, and Tiophene

molecule	atom A	N_A^{HOMO}	f_A^-	$f_A^-(\Delta N=-1)$	$f_A^-(\Delta N=-0.01)$	N_A^{LUMO}	f_A^+	$f_A^+(\Delta N=1)$	$f_A^+(\Delta N=0.01)$
CO	C	0.91	0.81	0.71	0.74	0.76	0.54	0.79	0.74
	O	0.09	0.19	0.29	0.26	0.24	0.46	0.21	0.26
HCN	H	0.02	0.17	0.16	0.18	0.00	0.20	0.11	0.12
	C	0.14	0.57	0.47	0.42	0.58	0.45	0.66	0.60
	N	0.84	0.26	0.36	0.40	0.42	0.34	0.23	0.28
H_2CO	C	0.05	−0.05	0.16	0.15	0.67	0.17	0.48	0.45
	O	0.70	0.63	0.40	0.40	0.33	0.51	0.23	0.26
	H	0.12	0.21	0.22	0.23	0.00	0.16	0.14	0.14
pyrrole	N	0.01	0.15	0.01	0.00				
	C_α	0.37	0.20	0.19	0.18				
	C_β	0.12	0.15	0.09	0.10				
furane	O	0.00	0.13	0.06	0.05				
	C_α	0.36	0.21	0.18	0.15				
	C_β	0.14	0.12	0.11	0.12				
tiophene	S	0.01	0.19	0.19	0.18				
	C_α	0.38	0.16	0.15	0.14				
	C_β	0.12	0.12	0.07	0.11				

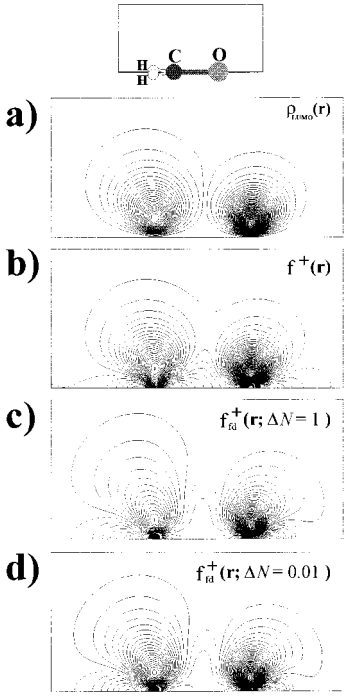

Figure 5. $f^+(\mathbf{r})$ FF plots for H_2CO. The diagrams correspond to the cut perpendicular to the molecular plane along the C−O bond.

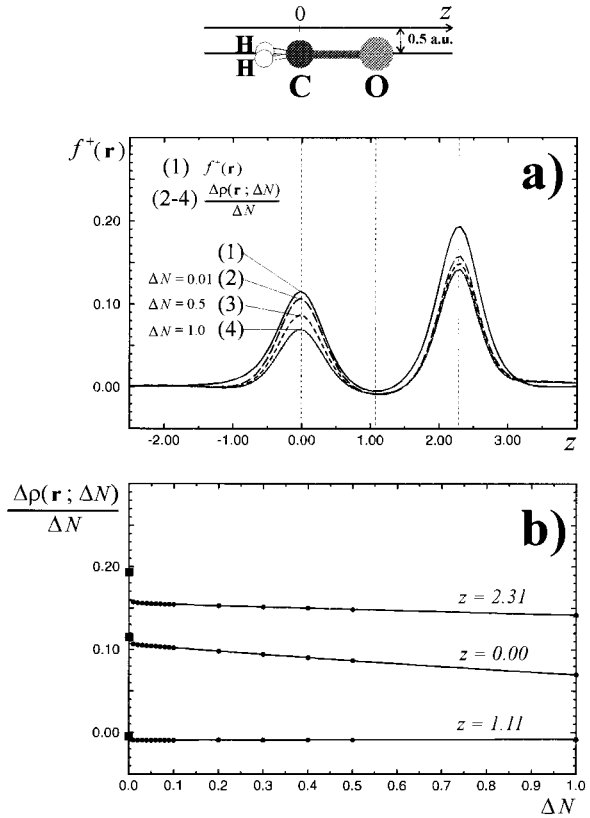

Figure 6. Illustrative profiles (panel a) from the corresponding cuts of Figure 5, along the probing line parallel to the C−O bond, 0.5 au above the molecular plane. Panel b tests the convergence of the finite difference FF values with the size of the populational displacement $0 < \Delta N \leq 1$ at the three indicated positions along the profile line; the corresponding differential estimates from the present approach are represented by the full squares in the $\Delta N \rightarrow 0$ limit. A similar convention is adopted in Figure 8.

of σ participation and basically no π component on nitrogen. One also detects a stronger $\alpha-\beta$ polarization in the latter case, which localizes the changes in density mostly on the α carbon.

Comparison with Finite Difference Predictions. It follows from our illustrative results that there are substantial quantitative differences between the corresponding differential and finite difference FF. It is observed (see panels c and d in Figures 1−5 and 7) that for $\Delta N < 0$, the magnitude of the finite difference shift in the number of electrons has a minor effect upon the FF pattern (e.g., Figures 2, 4, and 7). The sensitivity of the f_{fd} maps with respect to the magnitude of the $\Delta N > 0$ displacement appears to be somewhat higher (e.g., Figures 1 and 3); the smaller ΔN is seen to produce maps more similar to the differential counterparts (compare panels b and d of Figures 1, 3, and 5).

A more detailed comparison between the differential and finite difference FF values for formaldehyde is presented in Figures 6 and 8. The profiles of the differential and finite difference FF for selected ΔN values are shown in panels a of the figures, while the convergence of the FF values for representative points along the specified z-axes, indicated by the broken lines on panels a, are compared in panels b. In Figure 6a the following trend can be detected: with a decrease in the ΔN magnitude, the f_{fd} profile approaches the differential one. However, in Figure 8a, where all fd profiles are practically identical, a weak reverse trend is observed; these fd profiles reproduce well the corresponding differential plot in the dominating oxygen region.

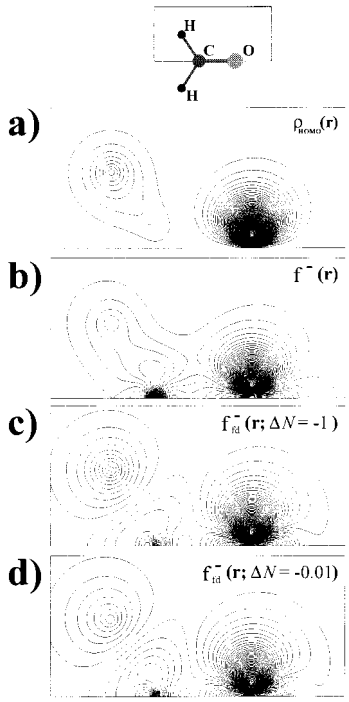

Figure 7. Contour maps in the molecular plane of the $f^{-}(\mathbf{r})$ FF for H_2CO.

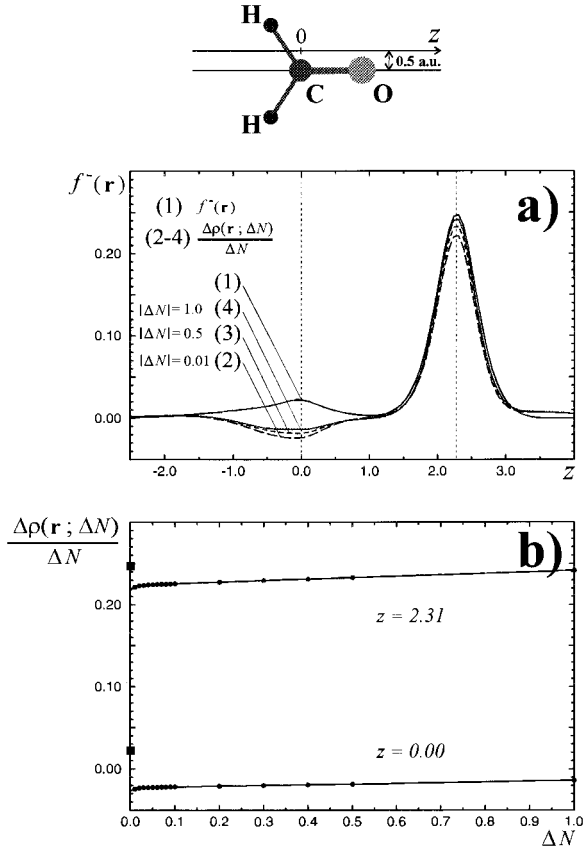

Figure 8. Illustrative profiles (panel a) from the corresponding cuts of maps shown in Figure 7 in the molecular plane along the line parallel to and 0.5 au above the C−O bond. Again, panel b tests the convergence of the finite difference values at the two indicated positions along the profile line.

A reference to Figures 6b and 8b shows that the $\Delta N \rightarrow 0$ intercepts, which can be considered as the "exact" reference values, are slightly different from the differential data (black

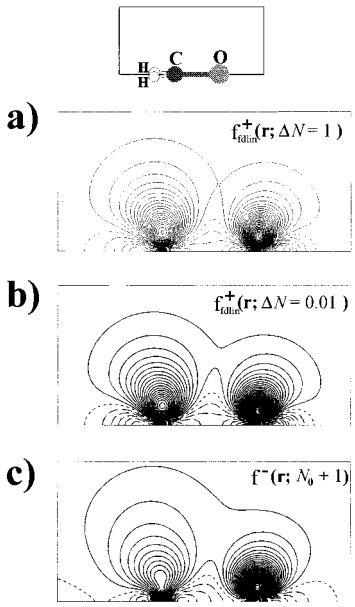

Figure 9. Linearly projected *nucleophilic* finite difference FF for the neutral formaldehyde: $\Delta N = 1$ (a) and $\Delta N = 0.01$ (b). Panel c shows the *electrophilic* differential FF for the molecular anion.

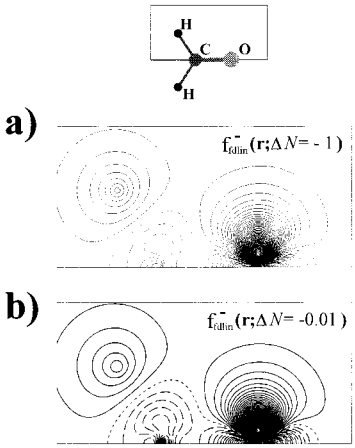

Figure 10. Linearly projected *electrophilic* finite difference FF for the neutral formaldehyde: $\Delta N = -1$ (a) and $\Delta N = -0.01$ (panel b).

squares). This deviation is a manifestation of the error introduced by the approximation of eq 20. Namely, the nonlinear terms in eq 31 should be negligible for very small ΔN. We have checked this numerically by generating the $f_{\mathrm{fdlin}}(\mathbf{r})$ values at all five points for $|\Delta N| = 0.01$; the results were practically indistinguishable from the standard finite difference approach including nonlinear terms. The importance of such contributions is additionally tested for formaldehyde in Figures 9 and 10. A comparison between the linear fd FF contributions for $|\Delta N| = 1$ (panels a) and $|\Delta N| = 0.01$ (panels b) shows that one can indeed obtain quite realistic FF patterns using the f_{fdlin} approach applied to a single-electron displacement. An inspection of the pairs of figures (Figures 5c and 9b) and (Figures 7c and 10b) (comparing diagrams—the first, for which the nonlinear changes do not vanish, with the second, for which these contributions are not present), indicates that the nonlinear terms do indeed distort the reference patterns at $|\Delta N| = 1$.

Therefore, should one have the orbital relaxation option available, the $f_{\mathrm{fdlin}}(\mathbf{r})$ functions (eq 33) can be recommended as the ones providing a more realistic finite difference estimate directly linked to the corresponding differential function.

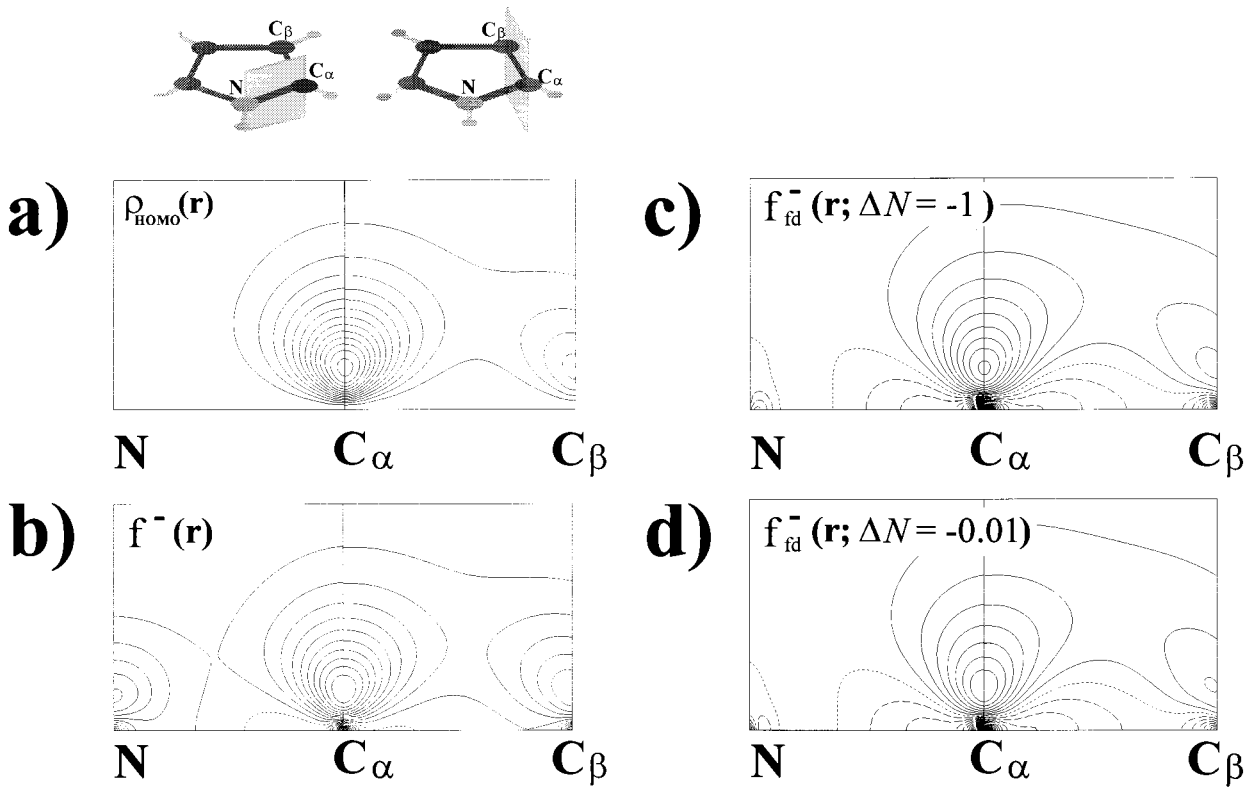

Figure 11. Same as in Figure 2 for pyrrole. The four diagrams combine the contour maps in the two cutting planes shown in the perspective plots preceding the four panels.

A given positive, finite ΔN displacement of the neutral molecule is equivalent to the complementary negative ΔN shift of the anion. One could expect, therefore, that the nucleophilic FF of the neutral system should resemble the electrophilic FF of the negatively charged species. This conjecture is tested in Figure 9, where the differential electrophilic Fukui function for the formaldehyde anion (panel c) is displayed. When compared with the nucleophilic counterpart of the neutral molecule (see Figure 5b or 9b), this map indeed exhibits a strong resemblance to the reference nucleophilic function of formaldehyde. As seen in the figures, both functions strongly resemble the LUMO density (Figure 5a). This should be expected on the basis of the physical interpretation of this orbital, since the LUMO of the neutral system indeed describes the ground state of an added electron in the effective field of the nuclei and the remaining electrons.

Atomic Discretization and Reactivity Trends. The "coarse-grained" resolution of the local, "fine-grained" FF into the relevant FF indices, e.g., in the AIM discretization, provides a convenient basis for interpreting the reactivity preferences in large molecular systems. In Table 1, we have listed the Mulliken-type (eq 16) condensed FF indices obtained from all local functions reported in the present work, except for the linearly projected fd FF.

The f^- part of the table, grouping the electrophilic FF numbers of constituent atoms, shows that the location of an electrophilic attack on CO, H_2CO, and pyrrole is correctly predicted from all Fukui function indices; they are in agreement with the selectivity conjectures based on both the number and ranges of the equidistant local FF contours of Figures 2, 7, and 11. The discrepancy observed in the HCN case, where the local FF plots [panels b and d of Figure 4] and the frontier orbital density indicate nitrogen as the preferred location of an electrophilic attack, is due to a cancellation of the positive and negative FF contributions to the FF indices within the heavy atoms.

For CO and HCN the nucleophilic FF numbers correctly predict the carbon atom as the preferred position for a nucleophilic attack. The formaldehyde condensed FF results are somewhat surprising. Namely, the immediate impression following an inspection of contours in Figure 5 seems to indicate the carbon as the favored electrophilic (electron accepting) site of formaldehyde in all approximations examined. Indeed, the same conclusion follows from both the rigid (frontier) and the finite difference condensed FF data. Therefore, it comes as a surprise that the condensed nucleophilic FF index obtained from the present, differential approach identifies oxygen as the maximum condensed FF site. This observation provides an example of the known deficiency of the Mulliken-type AIM discretization in the atomic orbital space, which often generates unphysical condensed charge distribution and condensed FF data, particularly in the extended basis sets including very diffused orbitals and polarization functions. The difficulties in obtaining the realistic net charges from the population analysis schemes are amplified in the FF case, since electron density is positive everywhere, while FF exhibits both negative and positive values, thus giving rise to a partial cancellation of the local contributions to the condensed atomic indices. Therefore, probing reactivity trends directly through FF maps should in principle be preferred over that of using the corresponding discretized AIM information.

The electrophilic FF maps for pyrrole shown in Figure 11 provide a comparison for a larger molecular system, the reactivity preferences of which (toward an electrophilic attack) has been the subject of theoretical investigations.[35−37] Both the electrostatic potential of a molecule and the charge distribution among the ring carbons slightly favor the β-substitution.[35,36] It has been found that the condensed FF indices from the semiempirical hardness matrix in atomic resolution correctly identify the α-carbons as the preferred sites for electrophilic substitution.[37] A reference to all local FF estimates, both

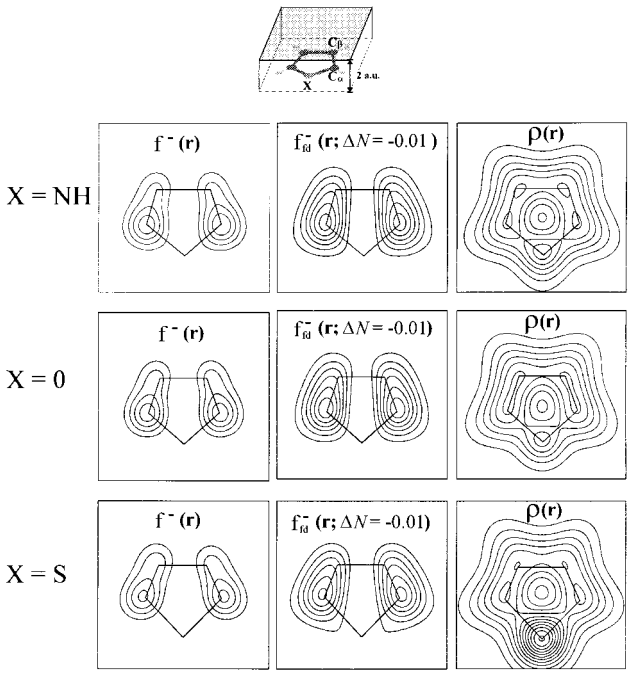

Figure 12. Contour diagrams of the electrophilic differential and fd FF for pyrrolle, furane, and tiophene; the last column shows the corresponding maps of the electron density in the same cut 2 au above the molecular plane. The contour increments are 0.001 au in the FF part and 0.005 au in the electron density plots.

differential and finite difference, provides additional support for this conclusion; the same strong α-preference follows from all condensed FF indices listed in Table 1.

In Figure 12 we have displayed the contour diagrams of the differential and the $\Delta N = -0.01$ fd FF, as well as the electron density for pyrrole, furane, and tiophene, plotted in the section 2 au above the ring plane. This cut has been selected to probe the selectivity of the electrophile approach to the π-electron system, which eventually determines the preference for the electrophilic substitution. It follows from the figure that the electronic density at this distance from the ring plane practically does not descriminate between α- and β-carbons. In the tiophene case, however, the large electron density on sulfur may indicate that the electrophile should approach the molecule on this site, thus facilitating the eventual substitution on the nearby α-carbon. A similar mechanism has been proposed for furane,[35] where the electophile should be strongly attracted by the proton-stabilizing basin of negative electrostatic potential near oxygen. The preference for the substitution reaction at this distance is clearly seen in all FF diagrams in Figure 12 (see also Figure 11), thus demonstrating the utility of the FF as a criterion for predicting subtle reactivity trends and validating the approximation adopted in the proposed algorithm.

A reference to the condensed FF indices for furane in Table 1 shows that in all approximations the α-carbon is predicted as the preferred substitution site. In the tiophene case, however, the prelimanary attack on sulfur is diagnosed in all cases, owing to FF contributions closer to the ring plane, which are missing in the cuts of Figure 12.

5. Concluding Remarks

The present work reports a single KS run determination of the approximate relaxed FF for molecular systems, for both electron withdrawal (electrophilic) and addition (nucleophilic) displacements. The proposed scheme requires the full complement of the two-electron integrals generated in typical SCF MO calculations, which are also availiable in some implementations of the KS method. The illustrative applications of the new algoritm demonstrate that it generates FF patterns adequate for probing the reactivity trends on the basis of the FF criterion of Parr and Yang.[1,2] The corresponding finite difference estimates require at least two KS calculations, including the relevant ionic ground state, which is sometimes difficult to converge, particularly for the anion. The differential FF predictions have been compared with the reference finite difference functions in the $|\Delta N| \rightarrow 0$ limit and the conventional fd FF for $|\Delta N| = 1$, for a series of simple molecules and selected five-membered heterocycles. An algorithm for removing the nonlinear terms in the fd approximation has also been proposed. The reactivity conjectures from the local FF and the condensed atomic indices have been compared, showing that atomic discretization may alter the predicted reactivity trends.

The fd FF for a single electron displacement sometimes give rise to wrong predictions about reactivity preferences (see, for example, Figure 3c). In the present work we have demonstrated, however, that both the differential and the $|\Delta N| = 0.01$ FF are quite reliable in this respect; the same is true in the f_{fdlin} approach corresponding to $|\Delta N| = 1$, in which the spurious nonlinear contributions are removed. Therefore, we can recommend FF obtained from all these schemes as adequate diagnostic tools for probing trends in chemical reactivity. A comparison between the differential FF and their fd counterparts shows quite convincingly that the present algorithm, based on eqs 17, 18, and 20, reproduces all major features of the fd FF diagrams and leads to correct reactivity predictions.

The question naturally arises about the effects neglected in the present approximation. Obviously, the Fukui function concept does not represent an observable, so a direct comparison with "experimental" reference function is not available. We believe that a practical proposition is to confront the *reactivity predictions* of the present approach with those known from experiment and resulting from other methods, since the Fukui function has indeed been intended as the reactivity concept. Although a comparison of the differential and fd FF has been found to be generally favorable, as far as both the dominating features and reactivity inferences are concerned, it cannot evaluate the observed differences. Another perspective from which one could pragmatically evaluate the FF algorithms is the computational complexity. As we have already argued, the adopted approximation neglects only a part of the electron exchange−correlation effects. Moreover, from the practical point of view, it does not lead to a qualitative increase in the computational effort in comparison with the standard KS calculations. Clearly, going beyond this approximation is possible, but it would only generate yet higher accuracy of this inherently qualitative reactivity index.

The *N*-derivative of the exchange−correlation potential is important for generating the *N*-discontinuity effects at an integer number of electrons.[11] However, the present approach does recognize them by a proper identification of the frontier orbital contributions for $\Delta N < 0$ and $\Delta N > 0$, respectively. Therefore, one can expect that the major relaxational effects are indeed realistically accounted for in the proposed algorithm.

The present work represents the KS extension of the recently published *Hartree−Fock* (HF) scheme for determining FF.[27] We would like to stress, however, the following basic difference between the two approaches. Namely, contrary to the Kohn−Sham theory, the identification of the HOMO energy as the chemical potential level in the Hartree−Fock theory is only an approximate one. For example, in transition metal complexes

the fractionally occuppied HF orbitals often lie below the HOMO level, thus making it impossible to predict a priori which orbital will accept the additional electron. Such ambiguity does not exist in the KS theory, where the only orbitals changing their occupations (*active MO*) are uniquely identified as the frontier orbitals relevant for the electron inflow/outflow to/from the system under consideration. Therefore, the FF predictions from HF theory will be similar to the less arbitrary KS results only in those cases, where the active orbitals of the HF approach, if appropriately identified, are similar to the frontier orbitals of the KS theory. Thus, the KS FF scheme, even that using approximate algorithm for the orbital relaxation, may prove to be a more reliable basis for reactivity predictions in general molecular systems.

Acknowledgment. This work was partly supported by a research grant from the State Committee for Scientific Research in Poland and by the Flemish−Polish Scientific Cooperation Program. One of the authors (A.M.) also acknowledges a fellowship from the Foundation for Polish Science.

References and Notes

(1) Parr, R. G.; Yang, W. *J. Am. Chem. Soc.* **1984**, *106*, 4049. Yang, W.; Parr, R. G. *Proc. Natl. Acad. Sci. U.S.A.* **1985**, *82*, 6723.

(2) Parr, R. G.; Yang, W. *Density Functional Theory of Atoms and Molecules*; Oxford University Press: New York, 1989 and references therein.

(3) Nalewajski, R. F.; Korchowiec, J. *Charge Sensitivity Approach to Electronic Structure and Chemical Reactivity*; World-Scientific: Singapore, 1997 and references therein. Nalewajski, R. F.; Korchowiec, J.; Michalak, A. In *Topics in Current Chemistry, Vol. 183: Density Functional Theory IV—Theory of Chemical Reactivity*; Nalewajski, R. F., Ed.; Springer-Verlag, Heidelberg, 1986; p 25.

(4) Cohen, M. H. In *Topics in Current Chemistry Vol. 183: Density Functional Theory IV—Theory of Chemical Reactivity*; Nalewajski, R. F., Ed.; Springer-Verlag: Heidelberg, 1986; p 143.

(5) Parr, R. G.; Pearson, R. G. *J. Am. Chem. Soc.* **1983**, *105*, 7512.

(6) Nalewajski, R. F. *J. Phys. Chem.* **1985**, *89*, 2831; *Z. Naturforsch.* **1988**, *43a*, 65; *J. Phys. Chem.* **1989**, *93*, 2658; *Acta Phys. Pol.* **1990**, *A77*, 817; *Int. J. Quantum Chem.* **1994**, *49*, 675. Nalewajski, R. F.; Koniński, M. *Acta Phys. Pol.* **1988**, *A74*, 255.

(7) Berkowitz, M.; Parr, R. G. *J. Chem. Phys.* **1988**, *88*, 2554.

(8) Sen, K. D., Ed. *Structure and Bonding, Vol. 80: Chemical Hardness*; Springer-Verlag: Berlin, 1993 and references therein.

(9) Nalewajski, R. F. In *Proceedings of a NATO ASI on Density Functional Theory*, Il Ciocco, August 16−27, 1993; Dreizler, R. M., Gross, E. K. U., Eds.: Plenum: New York, 1995; p 339.

(10) Nalewajski, R. F. In *Developments in the Theory of Chemical Reactivity and Heterogeneous Catalysis*, Proceedings of the International Workshop "The Activated Complex in Heterogeneous Catalysis", Leuven, May 30−31, 1996; Mortier, W. J., Schoonheydt, R., Eds.; Research Signpost: Trivandrum, 1998; in press.

(11) Gyftopoulos, E. P.; Hatsopoulos, G. N. *Proc. Natl. Acad. Sci. U.S.A.* **1968**, *60*, 786. Perdew, J. P.; Parr, R. G.; Levy, M.; Balduz, J. L. *Phys. Rev. Lett.* **1982**, *49*, 1691. Perdew, J. P. In *Density Functional Methods in Physics*; Dreizler, R. M., da Providencia, J., Eds.; NATO ASI Series B123: Plenum Press: New York, 1985; p 265. See also the following. van Leeuwen, R; Gritsenko, O. V.; Baerends, E. J. In *Topics in Current Chemistry, Vol. 180: Density Functional Theory I—Functionals and Effective Potentials*; Nalewajski, R. F., Ed.; Springer-Verlag: Heidelberg, 1986; p 107.

(12) Sanderson, R. T. *J. Am. Chem. Soc.* **1952**, *74*, 272. Sanderson, R. T. *Chemical Bonding and Bond Energy*; Academic Press: New York, 1976.

(13) Parr, R. G.; Donnelly, R. A.; Levy, M.; Palke, W. E. *J. Chem. Phys.* **1978**, *68*, 801.

(14) Korchowiec, J.; Gerwens, H.; Jug, K. *Chem. Phys. Lett.* **1994**, *222*, 58.

(15) Nalewajski, R. F. *Int. J. Quantum Chem.* **1995**, *56*, 453; *Int. J. Quantum Chem.* **1997**, *61*, 181.

(16) Nalewajski, R. F.; Korchowiec, J. *J. Mol. Catal.* **1996**, *112*, 167. Nalewajski, R. F.; Michalak, A. *J. Phys. Chem.* **1996**, *100*, 20076; *J. Phys. Chem. A* **1998**, *102*, 636.

(17) Nalewajski, R. F.; Korchowiec, J. *J. Mol. Catal.* **1989**, *54*, 324.

(18) (a) Nalewajski, R. F. *Int. J. Quantum Chem.* **1998**, *69*, 591. (b) Nalewajski, R. F. *Pol. J. Chem.* **1998**, *72*, 1763.

(19) Nalewajski, R. F. In *Structure and Bonding, Vol. 80: Chemical Hardness*; Sen, K. D., Ed.; Springer-Verlag: Berlin, 1993; p 115.

(20) Baekelandt, B.; Mortier, W.; Schoonheydt, R. A. In *Structure and Bonding, Vol. 80: Chemical Hardness*; Sen, K. D., Ed.; Springer-Verlag: Berlin, 1993; p 187.

(21) Gazquez, J. L.; Vela, A.; Galwan, M. In *Structure and Bonding, Vol. 66: Electronegativity*; Sen, K. D., Ed.; Springer-Verlag: Heilderberg, 1987; p 79.

(22) Komorowski, L.; Lipiński, J. *Chem. Phys.* **1991**, *157*, 45.

(23) Ciosłowski, J.; Mixon, S. T. *J. Am. Chem. Soc.* **1991**, *113*, 4142.

(24) Chattaraj, P. K.; Cedillo, A.; Parr, R. G. *J. Chem. Phys.* **1995**, *103*, 7645.

(25) Senet, P. *J. Chem. Phys.* **1996**, *105*, 6471. Senet, P. *J. Chem. Phys.*, in press.

(26) De Proft, F.; Liu, S.; Geerlings, P.; Parr, R. G. *Pol. J. Chem.* **1998**, *72*, 1737.

(27) Balawender, R.; Komorowski, L. *J. Chem. Phys.* **1998**, *109*, 5203.

(28) De Proft, F.; Martin, J. M. L.; Geerlings, P. *Chem. Phys. Lett.* **1996**, *265*, 400. Geerlings, P.; De Proft, F.; Martin, J. M. L. In *Recent Developments in Density Functional Theory*; Seminario, J., Ed.: Elsevier: Amsterdam, 1996; p 773.

(29) Nalewajski, R. F. *Int. J. Quantum Chem.* **1991**, *40*, 265.

(30) Nalewajski, R. F.; Parr, R. G. *J. Chem. Phys.* **1982**, *77*, 399.

(31) Kohn, W.; Sham, L. J. *Phys. Rev.* **1965**, *140A*, 1133.

(32) Hohenberg, P.; Kohn, W. *Phys. Rev.* **1964**, *136B*, 864.

(33) The LCGTO-LSD-DF program deMon, developed by A. St.-Amant and D. R. Salahub at the University of Montreal, Canada.

(34) Dupuis, M.; Spangler, D.; Wendoloski, J. J. *National Resource for Computations in Chemistry, Software Catalog*; University of California, Berkeley, 1980. Schmidt, M. W.; Baldridge, K. K.; Boatz, J. A.; Jensen, J. H.; Koseki, S.; Gordon, M. S.; Nguyen, K. A.; Windus, T. J.; Elbert, S. T. *QCPE Bull.* **1990**, *10*, 52. *General Atomic and Molecular Electronic Structure System GAMESS: User's Guide*; North Dakota State University, Fargo and Iowa State University, Ames.

(35) Politzer, P.; Weinstein, H. *Tetrahedron* **1975**, *31*, 915 and references therein.

(36) Nalewajski, R. F.; Koniński, M *J. Mol. Struct.: THEOCHEM* **1988,** *165*, 365.

(37) Nalewajski, R. F.; Korchowiec, J. *Acta Phys. Pol.* **1989**, *A76*, 747; *Croat. Chem. Acta* **1989**, *62*, 603.